Effect of Stitch Seam Orientation on the Mode I Fracture Energy of Stitched Composites

Aditya Shah[1] and Rani W. Sullivan[2]
Mississippi State University, Mississippi State, MS, 39759, USA

Andrew E. Lovejoy[3] and Daniel A. Drake[4]
NASA Langley Research Center, Hampton, VA, 23681, USA

The use of carbon fiber-reinforced polymer (CFRP) composites has increased in the aerospace industry mainly due to their high stiffness and strength-to-weight ratios. However, these composites have low interlaminar strength that can result in delaminations when subjected to out-of-plane deformations. Through-the-thickness reinforcement, such as stitching, has been shown to increase interlaminar properties, resulting in improved crack-resistant characteristics. In this study, the influence of stitch seam orientation on the Mode I fracture energy, or strain energy release rate (SERR), of CFRP composites that are stitched using a one-sided modified chain stitching technique is investigated. The Mode I SERR was determined for stitched double cantilever beam specimens. A digital image correlation system was used to acquire surface strain measurements, and fracture surfaces were analyzed via an optical microscope. The results of the study indicated that SERR is dependent on stitch seam orientation. Therefore, the expected crack direction is crucial in designing stitch patterns within integrally stiffened composite structures.

I. Nomenclature

b	=	Width of the specimen
J_I	=	Mode I strain energy release rate
P	=	Applied load
θ	=	Angle at load application point

II. Introduction

The use of polymer matrix composites has been increasing in the aerospace, marine, and automotive industries in recent years. These composites offer superior stiffness, high strength-to-weight ratio, and are highly tailorable. However, carbon fiber composites have low interlaminar strength, which can result in delaminations when subjected to high interlaminar stresses [1]. Delamination is often due to low-velocity impacts such as a tool drop on a composite part, or other similar out-of-plane loading conditions [2–5]. Various through-thickness reinforcement methods, such

[1] Graduate Research Student, Department of Aerospace Engineering, Mississippi State University, MS 39762, Student Member.
[2] Professor and Department Head, Department of Aerospace Engineering, Mississippi State University, MS 39762, Associate Fellow.
[3] Senior Research Aerospace Engineer, Structural Mechanics and Concepts Branch, Associate Fellow AIAA.
[4] Senior Research Aerospace Engineer, Structural Mechanics and Concepts Branch, Member AIAA.

as z-pinning and stitching, have been used to improve interlaminar fracture toughness [6–10]. As shown in various studies [1,11], stitching can increase the strain energy release rate (SERR) of composite materials for both Mode I and Mode II. The stitches act as bridging elements between two opposing crack faces, thereby enhancing the overall interlaminar properties [11,12].

Traditional stitching techniques, such as the chain stitch or lock stitch, require access to both sides of the preforms, which can lead to difficulty stitching complex geometries such as flanges, stiffeners, and wind turbine blades [13]. One-sided stitching using stitching styles such as the modified chain stitch and tufting are preferred as these do not require access to the underside of the preform [14–16]. The ability to stitch from one side of the preform increases the complexity and size of the preform that can be stitched and allows for the unitization of structural elements that contain biaxial stiffening features [16–18]. For the one-sided modified chain stitching technique, an insertion needle inserts the stitching thread into a dry carbon preform, and a catcher needle then pulls the thread from the underside to the topside of the preform, which forms the modified chain stitch. Tooling with internal reliefs to account for needle travel is necessary to hold the dry carbon preforms while being stitched.

The effects of stitching on the Mode I SERR of stitched composites have been studied extensively [8, 19–23], but there are few studies investigating the influence of stitch orientation on the fracture behavior of stitched composites using the one-sided modified chain stitching technique [13]. The objective of this study is to explore the effects of stitch orientation of the modified chain stitch on fracture behavior and Mode I SERR.

III. Experimental Methodology

A. Composite Fabrication

Stitched double cantilever beam (DCB) specimens were fabricated from an infused carbon fiber/epoxy laminate of $[(90/0/0/90)]_{5s}$ configuration. Two dry non-crimp fabric (NCF) preforms of size 304.8 mm x 304.8 mm were stitched at NASA Langley Research Center with four rows of 250 mm length stitch paths with a 5 mm stitch pitch. All stitching was done using robotic single-sided modified chain stitching, which uses an insertion needle and a catcher needle, as shown in Fig. 1a. The insertion needle penetrates the dry perform at a 45º angle while the catcher needle penetrates the plies at 90º to pick up the sewing thread. Vectran™[*] thread of 1200 denier linear thread density with a polyvinyl alcohol (PVA) coating was used for all stitching. A Teflon™ film of 0.025 mm thickness and 70 mm length, placed at the midplane between plies 20 and 21, was used as the crack initiator. In the first panel (Fig. 2a), the insertion needle seam was in closer proximity to the crack initiator for each path, while in the second panel (Fig. 2b), the catcher needle seam was near the crack initiator.

The stitched dry preforms were fabricated using a vacuum-assisted resin transfer molding process using Hexflow-1078, an out-of-autoclave resin system; the laminates were cured using the temperature cycle shown in Fig. 3. After the curing process, the stitched panels were sectioned to obtain three DCB specimens with dimensions 280 mm x 25.4 mm x 7.8 mm for each stitch configuration. Each specimen contained the crack initiator and all four stitch paths for both stitch configurations. Piano hinges were bonded on the top and bottom ends of the sectioned specimens to provide loading attachment points for mechanical testing, as shown in Fig. 4. The through-thickness edges of the DCB specimens were speckle painted with flat protective enamel to obtain surface strain fields using digital image correlation (DIC).

The stitch orientation with respect to the crack propagation direction is shown in Fig. 5. The stitched DCB specimens in which the 90º catcher needle seam is the closest to the crack initiator are designated as CI-#, where # is the specimen number. The stitched DCB specimens in which the 45º insertion needle seam is the closest to the crack initiator are designated as IC-#. All three replicates of each specimen type were tested.

[*] The use of trademarks or names of manufacturers in this paper is for accurate reporting and does not constitute an official endorsement, either expressed or implied, of such products or manufacturers by the National Aeronautics and Space Administration.

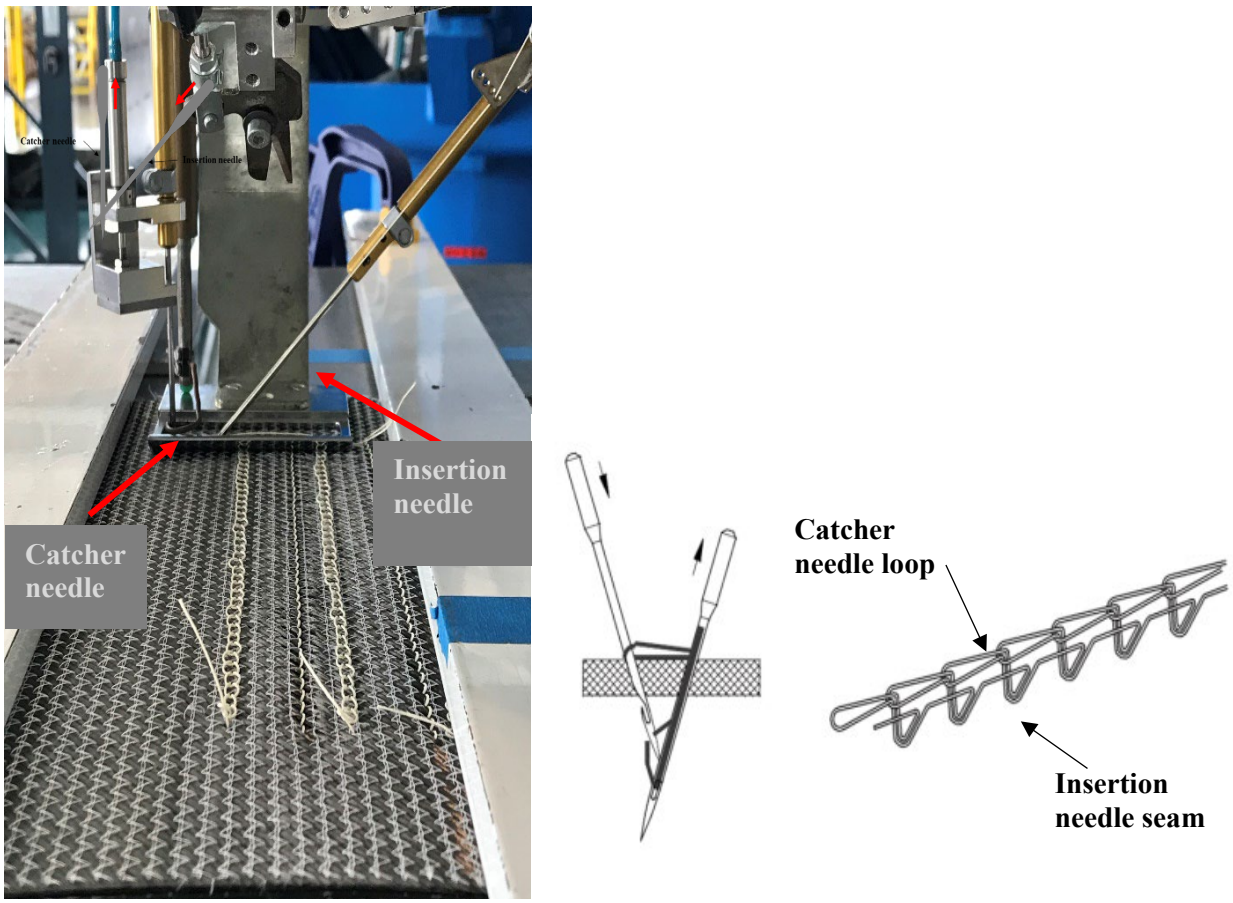

(a) (b)

Fig. 1 (a) One-sided stitching on a dry preform using a stitching robot and (b) one-sided stitching geometry [24]**.**

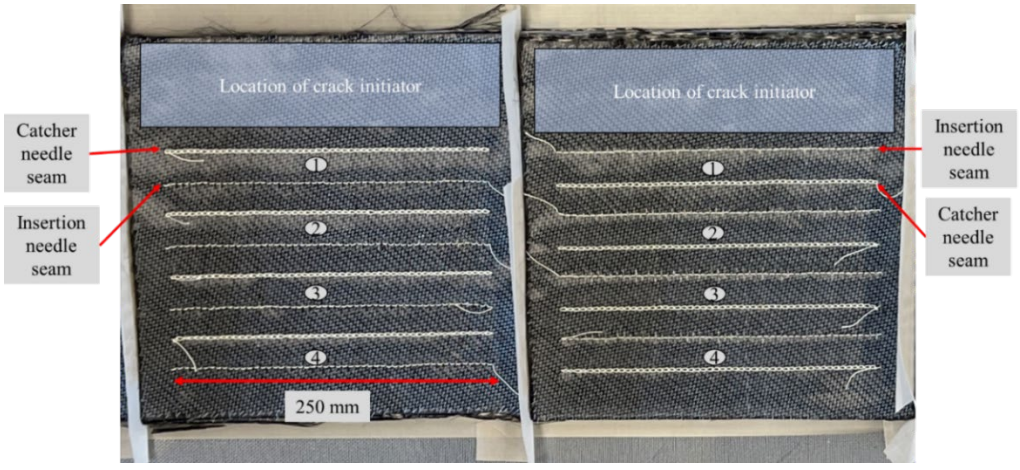

(a) (b)

Fig. 2 Modified chain stitching with (a) catcher seam closest to the crack initiator and (b) insertion seam nearest to the crack initiator.

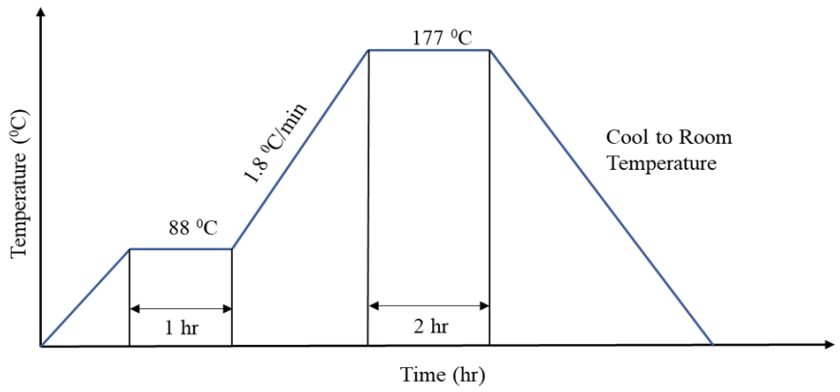

Fig. 3 Cure cycle temperatures used for the infused stitched preforms.

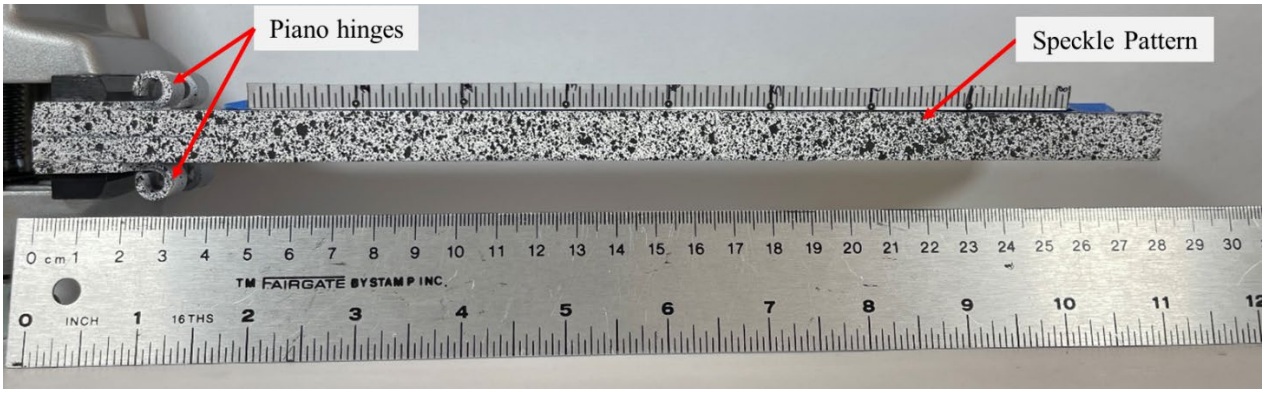

Fig. 4 DCB specimen with piano hinges and speckle pattern.

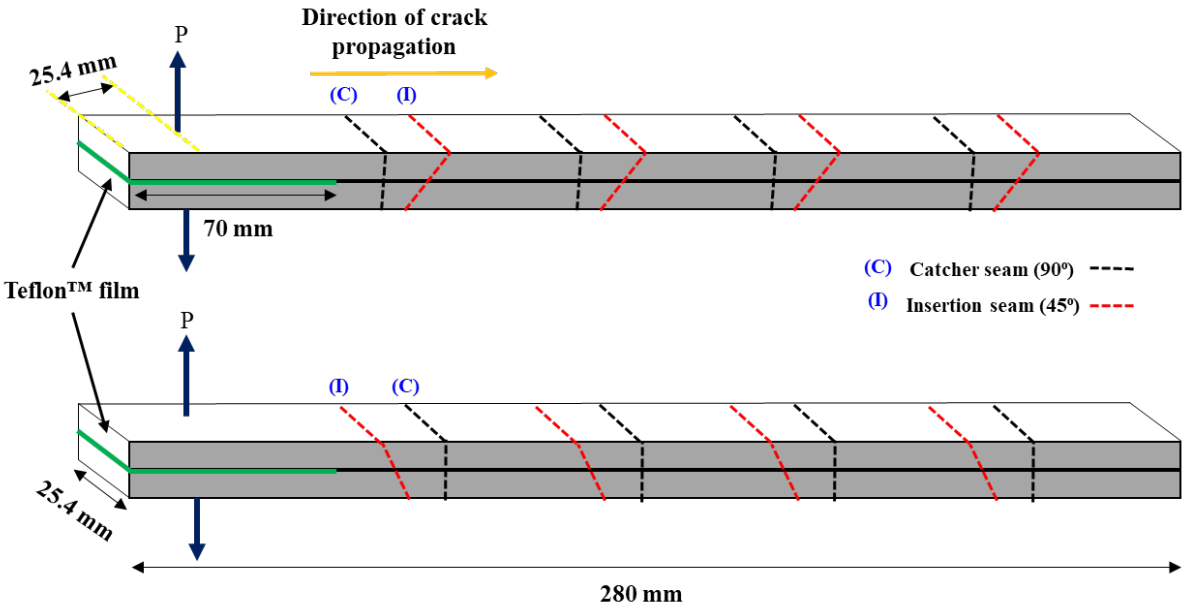

Fig. 5 DCB specimen with different stitch seam orientations.

B. Testing Methodology

The DCB specimens were tested in a hydraulic test frame using a 1 kN load cell. All tests were conducted under displacement control at a rate of 1 mm/min per the American Society for Testing and Materials (ASTM) ASTM D5528-13 standard, and the load and displacements were recorded at a 3 Hz sampling rate [25]. Surface strain fields from the sides of the specimens were acquired using an ARAMIS three-dimensional (3D) DIC system at a sampling rate of 3 Hz [26]. The DIC system had two 2.3-megapixel cameras for a stereoscopic setup to acquire 3D surface measurements. Additionally, two inclinometers were mounted on the top and bottom beam of the specimen using an additively manufactured rig to collect angle measurements, as shown in Fig. 6.

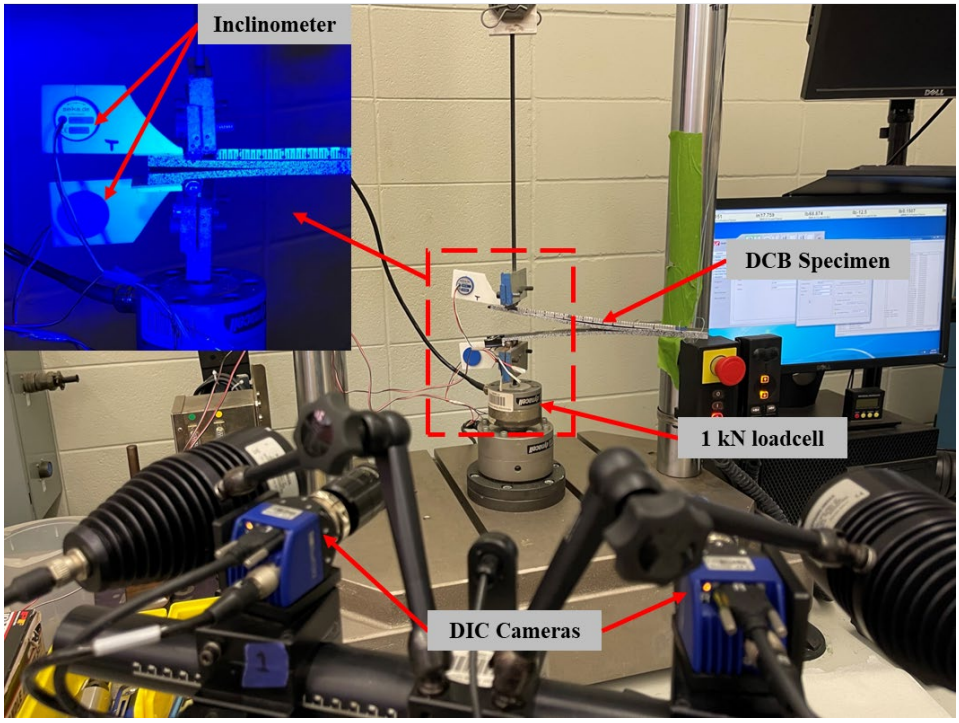

Fig. 6 DCB test setup.

IV. Strain Energy Release Rate

The SERR for each specimen was calculated using simplified analytical expressions based on the J-integral approach. The J-integral approach is based on integrating a contour integral near the crack tip field and the outer boundary of the specimen. Based on a slender double cantilever beam specimen with a uniform rectangular specimen, the J-integral expression for the opening mode I SERR is given as

$$\boldsymbol{J = \frac{2P\theta}{b}}, \tag{1}$$

where the applied load and width of the specimen are defined as $\boldsymbol{P}$ and $\boldsymbol{b}$, respectively. The term $\boldsymbol{\theta}$ is the measured angle at the load-application point [27]. The J-integral expression shown in Eq. (1) is independent of crack length. Additionally, the rotation at the load-application point is primarily influenced by the crack-root rotation and elastic foundation near the crack tip. Crack-root rotation correction does not need to be accounted for using Eq. (1). Under linear elastic conditions, Eq. (1) is equivalent to the Mode I interfacial fracture energy G_I using modified beam theory [28].

V. Results and Discussions

A. Load-Displacement Response

The load and applied displacement responses of the DCB specimens are shown in Fig. 7. Five distinct regions can be used to characterize the load-displacement response. Initially, the load-displacement response is linear as the specimen undergoes elastic deformation (region 1). At 146 ±6 N, the crack propagation begins through the unstitched region of the specimen, indicated by the slight decreases in load (region 2). The stitches arrest the crack growth, indicated by the large load increase (region 3). Once the load reaches a critical point (region 4), the stitches fail, resulting in an abrupt decrease in load (region 5). Post load drop in region 5, the next row of stitches arrests the crack, resulting in a slight increase in load similar to region 3 before the load drop due to stitch failure as the process is repeated.

In all specimens but specimen IC-3, single stitch row failure is overserved. In specimen IC-3, both the insertion and catcher stitch rows failed simultaneously, as shown by a single load drop at a higher displacement compared to two distinct load drops for successive stitch row failures at different displacements for other specimens. The initial failure load was similar for all specimens, but the failure load for the initial stitch row was higher in the CI specimens (90º catcher seam) than the IC specimens (45º insertion seam). Additionally, the CI specimens have a greater load-displacement slope when compared to the IC specimens at an applied displacement ranging from 4 mm to 10 mm. This increase in the load-displacement slope of the CI specimens could be associated with the orientation of the initial stitch that begins to bridge the delaminated interface, where the 90º stitches will begin to bridge prior to the 45º stitches for the CI specimens. In the IC specimens, the 45º stitches will begin to bridge prior to the 90º specimens, which may result in a lower load-displacement slope than the IC specimens. The average peak load of 285 N is about 12% higher for the CI specimens when compared to the 255 N average peak load for the IC specimens. The increase in maximum load may be a result of a lower load-carrying capacity of 45-degree stitches.

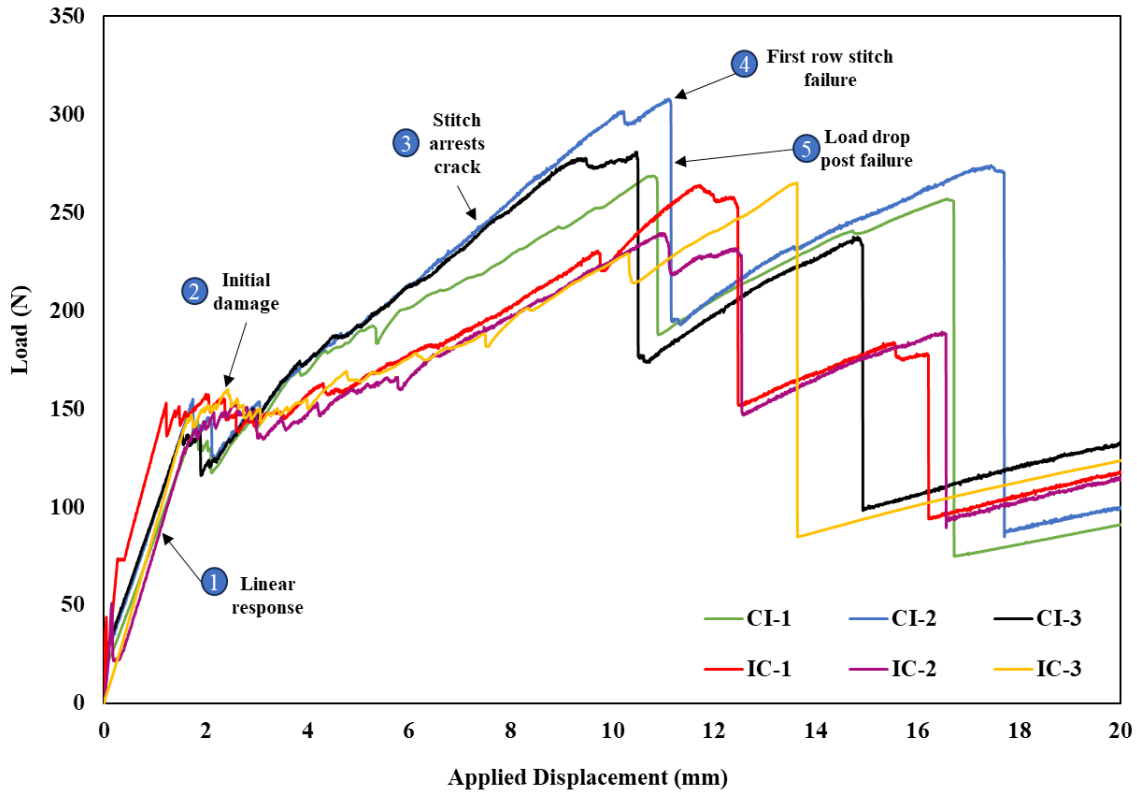

Fig. 7 Load-displacement response of the DCB specimens.

B. Strain Energy Release Rate

The calculated SERR is shown in Fig. 8. The initiation SERR for the unstitched region for both specimen types are similar, with an average value of all six specimens of 214 ± 10 J/m^2. The maximum SERR occurs before the first stitch row failure, followed by a drop in energy release rate attributed to the energy loss due to stitch failure. The average SERR for the catcher-seam failure in the CI specimens is 1810 J/m^{2,} which is approximately 15% higher than the average SERR observed in the IC specimens. The decrease in SERR in the IC specimens can be attributed to the lower shear load-carrying capacity of the insertion needle portion of the stitches. For both specimen types, the SERR values increase again, which can be attributed to the next stitch row arresting the crack. On average, the SERR at first stitch row failure for all specimens is approximately 154% greater than the average SERR at initiation, demonstrating the damage-arresting feature of the through-thickness stitching.

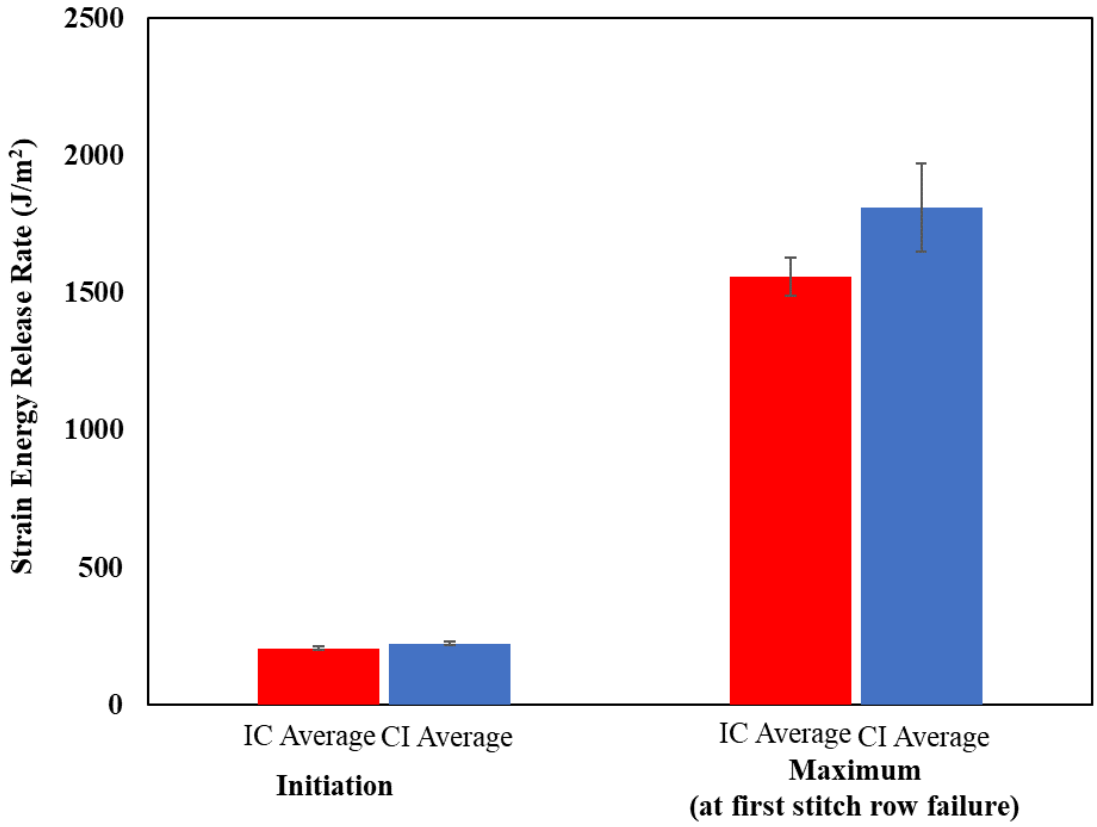

Fig. 8 SERR of the DCB specimens at initiation and first stitch failure.

C. Stitch Failure

In the IC specimens, the first row of stitches failed at the mid-plane at both the insertion and catcher seams. However, different failure mechanisms were observed for the CI specimens; some stitches failed due to pull-out, while others failed at the mid-plane. Interestingly, the stitches that failed due to pull-out were on the top half of the specimen during loading. An optical microscope image of a failed stitch due to pull-out failure is shown in Fig. 9a. the different stitch failure mechanisms observed in specimen CI-1 is shown in Fig. 9b.

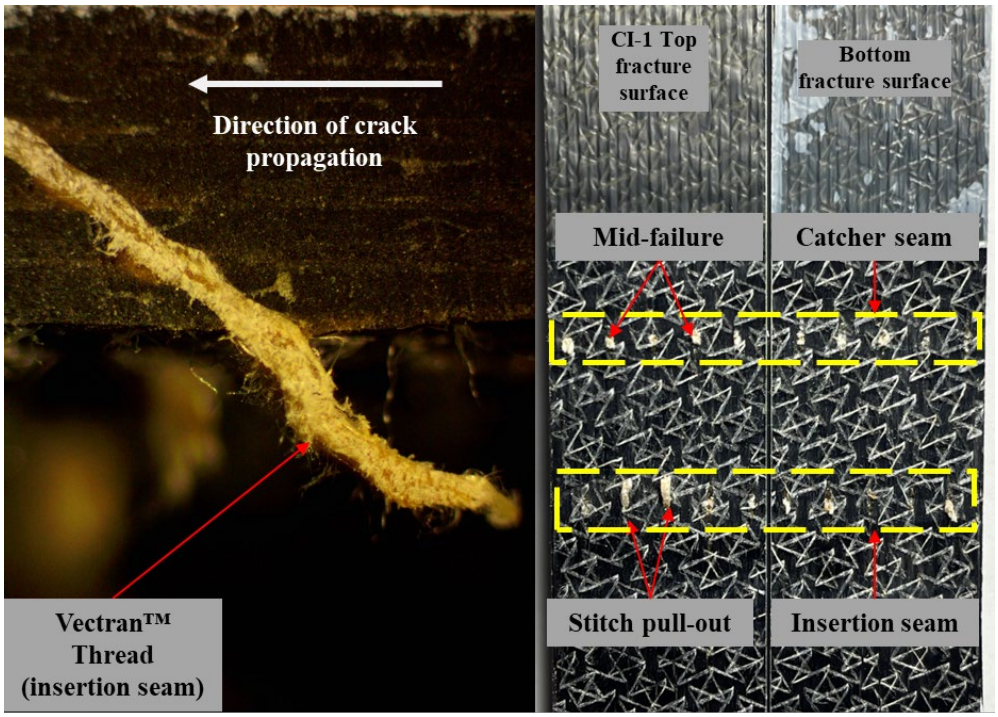

(a) (b)

Fig. 9 (a) Stitch failure due to pull-out in specimen CI-1 and (b) stitch failure in top and bottom fracture surface of specimen CI-1.

VI. Conclusions

In this study, the strain energy release rate (SERR) of one-sided stitched double cantilever beam (DCB) specimens with different seam orientations was calculated using the J-integral method. The through-thickness stitching shows excellent damage-arresting capabilities, with the average SERR associated with the stitches being significantly higher than SERR values in the unstitched region.

It was observed that the specimens in which the insertion seam followed the catcher seam (CI specimens) have an increase in SERR by about 15% compared to the specimens in which the catcher seam followed the insertion seam (IC specimens). The reduction in SERR can be attributed to the lower load-carrying capacity of the 45º stitches in the insertion seams as compared to the 90º stitches in the catcher seam. The load-displacement response of the specimens was typical of stitched specimens, in which significant increases in the measured load were recorded as the crack front progressed near a stitch row, and then when the stitches failed, the load decreased. Images of the fracture surfaces show different stitch failure mechanisms based on the stitch orientation. The stitches failed in the midplane for the IC specimens. In contrast, the CI specimens had multiple types of failure, such as stitch pull-out and midplane failures. The result of this research demonstrates that there are differences in SERR based on the stitch seam orientation with respect to the crack front. Thus, determining the expected load path and crack direction is crucial in designing stitched load-bearing structures, as the SERR can vary based on the stitch orientation.

Funding Sources

This work was supported by the NASA Langley Research Center under the Space Act Agreement (SAA1-32662) and the Federal Aviation Administration (FAA) (Award #: G00003737). The authors gratefully acknowledge the support from the Advanced Composites Institute's Marvin B. Dow Stitched Composites Development Center and the High-Performance Composite Materials Laboratory in the Department of Aerospace Engineering at Mississippi State University.

References

[1] Dransfield, K., Baillie, C., and Mai, Y.-W., "Improving the Delamination Resistance of CFRP by Stitching—a Review," *Composites Science and Technology*, Vol. 50, No. 3, 1994, pp. 305–317. https://doi.org/10.1016/0266-3538(94)90019-1

[2] Francesconi, L., and Aymerich, F., "Numerical Simulation of the Effect of Stitching on the Delamination Resistance of Laminated Composites Subjected to Low-Velocity Impact," *Composite Structures*, Vol. 159, 2017, pp. 110–120. https://doi.org/10.1016/j.compstruct.2016.09.050

[3] Shah, A., and Sullivan, R. W., "Out-Of-Plane Displacements of Composite DCB Specimens Using Embedded Optical Fiber Strains," *Proceedings of the American Society for Composites (ASC) 37th Annual Technical Conference,* Tuscon, AZ, 2022. https://doi.org/https:/doi.org/10.12783/asc37/36397

[4] Drake, D. A., and Sullivan, R. W., "The Fracture Behavior of Stitched Sandwich Composites," Ph.D. Dissertation, Dept. of Aerospace Engineering, Mississippi State Univ., Starkville, Mississippi, 2021.

[5] Cantwell, W. J., and Morton, J., "The Impact Resistance of Composite Materials — a Review," *Composites*, Vol. 22, No. 5, 1991, pp. 347–362. https://doi.org/10.1016/0010-4361(91)90549-V

[6] Pegorin, F., Pingkarawat, K., Daynes, S., and Mouritz, A. P., "Influence of Z-Pin Length on the Delamination Fracture Toughness and Fatigue Resistance of Pinned Composites," *Composites Part B: Engineering*, Vol. 78, 2015, pp. 298–307. https://doi.org/10.1016/j.compositesb.2015.03.093

[7] M'membe, B., Gannon, S., Yasaee, M., Hallett, S. R., and Partridge, I. K., "Mode II Delamination Resistance of Composites Reinforced with Inclined Z-Pins," *Materials and Design*, Vol. 94, 2016, pp. 565–572. https://doi.org/10.1016/j.matdes.2016.01.051

[8] Shah, A., Drake, D., and Sullivan, R. W., "Fracture Toughness of Stitched CFRP Composites Using Optical Fiber Strains," *Proceedings of the American Society for Composites (ASC) 35th Annual Technical Conference,* Virtual, 2020. https://doi.org/10.12783/asc35/34860

[9] Drake, D. A., Sullivan, R. W., Clay, S. B., and DuBien, J. L., "Influence of Stitching on the Fracture of Stitched Sandwich Composites," *Composites Part A: Applied Science and Manufacturing*, Vol. 145, 2021. https://doi.org/10.1016/j.compositesa.2021.106383

[10] Jain, L. K., Dransfield, K. A., and Mai, Y.-W., "On the Effects of Stitching in CFRPs—II. Mode II Delamination Toughness," *Composites Science and Technology*, Vol. 58, No. 6, 1998, pp. 829–837. https://doi.org/10.1016/S0266-3538(97)00186-3

[11] Drake, D. A., Sullivan, R. W., Lovejoy, A. E., Clay, S. B., and Jegley, D. C., "Influence of Stitching on the Out-of-Plane Behavior of Composite Materials – A Mechanistic Review," *Journal of Composite Materials*, Vol. 55, No. 23, 2021, pp. 3307–3321. https://doi.org/10.1177/00219983211009290

[12] Mouritz, A. P., Leong, K. H., and Herszberg, I., "A Review of the Effect of Stitching on the In-Plane Mechanical Properties of Fibre-Reinforced Polymer Composites," *Composites Part A: Applied Science and Manufacturing*, Vol. 28, No. 12, 1997, pp. 979–991. https://doi.org/10.1016/S1359-835X(97)00057-2

[13] Plain, K. P., and Tong, L., "An Experimental Study on Mode I and II Fracture Toughness of Laminates Stitched with a One-Sided Stitching Technique," *Composites Part A: Applied Science and Manufacturing*, Vol. 42, No. 2, 2011, pp. 203–210. https://doi.org/10.1016/j.compositesa.2010.11.006

[14] Velicki, A., and Jegley, D., "PRSEUS Structural Concept Development," AIAA 2014-0259, *52nd Aerospace Sciences Meeting,* 2014. https://doi.org/10.2514/6.2014-0259

[15] Jegley, D. C., and Velicki, A., "Development of the PRSEUS Multi-Bay Pressure Box for a Hybrid Wing Body Vehicle," AIAA 2015-1871, *56th AIAA/ASCE/AHS/ASC Structures, Structural Dynamics, and Materials Conference*, January 2015.

[16] Bergan, A., Bakuckas, J. G., Lovejoy, A., Jegley, D., Linton, K., Neal, B., Korkosz, G., Awerbuch, J., and Tan, T.-M., "Full-Scale Test and Analysis Results of a PRSEUS Fuselage Panel to Assess Damage Containment Features," *Proceedings of the 2011 Aircraft Airworthiness and Sustainment Conference*, San Diego, 2011.

[17] Jegley, D. C., Przekop, A., Lovejoy, A. E., Rouse, M., and Wu, H.-Y. T., "Structural Response of a Stitched Composite Hybrid Wing Body Center Section," *Journal of Aircraft*, Vol. 58, No. 3, 2021, pp. 580–590. https://doi.org/10.2514/1.C035911

[18] Jegley, D. C., Rouse, M., Przekop, A., and Lovejoy, A. E., "The Behavior of a Stitched Composite Large-Scale Multi-Bay Pressure Box," NASA TM-2016-218972, Hampton, VA, 2016.

[19] Plain, K. P., and Tong, L., "The Effect of Stitch Incline Angle on Mode I Fracture Toughness - Experimental and Modelling," *Composite Structures*, Vol. 92, No. 7, 2010, pp. 1620–1630. https://doi.org/10.1016/j.compstruct.2009.11.027

[20] Mouritz, A., "Further Validation of the Jain and Mai Models for Interlaminar Fracture of Stitched Composites," *Composites Science and Technology*, Vol. 59, No. 11, 1999, pp. 1653–1662. https://doi.org/10.1016/S0266-3538(99)00027-5

[21] Jiang, T., Guan, Z., Li, Z., Liu, X., and Geng, K., "Experimental and Numerical Study on Mode I Interlaminar Fracture Toughness of Lightly Stitched Ceramic-Matrix Composites," *Results in Physics*, Vol. 19, 2020. https://doi.org/10.1016/j.rinp.2020.103422

[22] Velmurugan, R., and Solaimurugan, S., "Improvements in Mode I Interlaminar Fracture Toughness and In-Plane Mechanical Properties of Stitched Glass/Polyester Composites," *Composites Science and Technology*, Vol. 67, No. 1, 2007, pp. 61–69. https://doi.org/10.1016/j.compscitech.2006.03.032

[23] Solaimurugan, S., and Velmurugan, R., "Influence of In-Plane Fibre Orientation on Mode I Interlaminar Fracture Toughness of Stitched Glass/Polyester Composites," *Composites Science and Technology*, Vol. 68, Nos. 7–8, 2008, pp. 1742–1752. https://doi.org/10.1016/j.compscitech.2008.02.008

[24] Trabelsi, W., Michel, L., and Othomene, R., "Effects of Stitching on Delamination of Satin Weave Carbon-Epoxy Laminates under Mode I, Mode II and Mixed-Mode I/II Loadings," *Applied Composite Materials*, Vol. 17, No. 6, 2010, pp. 575–595. https://doi.org/10.1007/s10443-010-9128-0

[25] "Standard Test Method for Mode I Interlaminar Fracture Toughness of Unidirectional Fiber-Reinforced Polymer Matrix Composites," ASTM Standard. https://doi.org/10.1520/D5528-13

[26] "ARAMIS 3D Camera Systems," Retrieved 3 July 2021. https://www.gom.com/en/products/3d-testing/aramis-3d-camera, Accessed Jul. 3, 2021.

[27] Paris, A. J., and Paris, P. C., "Instantaneous Evaluation of J and C," *International Journal of Fracture*, Vol. 38, No. 1, 1988, pp. R19–R21. https://doi.org/10.1007/BF00034281

[28] Drake, D. A., and Sullivan, R. W., "Interfacial Fracture Energy of a Single Cantilevered Beam Specimen Using the J-Integral Method," *International Journal of Fracture*, Vol. 229, No. 2, 2021, pp. 185–194. https://doi.org/10.1007/s10704-021-00547-6